Earth and Planetary Science Letters 496 (2018) 168–177

Contents lists available at ScienceDirect

Earth and Planetary Science Letters

www.elsevier.com/locate/epsl

Sulfur isotopes in rivers: Insights into global weathering budgets, pyrite oxidation, and the modern sulfur cycle

Andrea Burke [a,b,*], Theodore M. Present [b], Guillaume Paris [b,c], Emily C.M. Rae [a], Brodie H. Sandilands [a], Jérôme Gaillardet [d,e], Bernhard Peucker-Ehrenbrink [f], Woodward W. Fischer [b], James W. McClelland [g], Robert G.M. Spencer [h], Britta M. Voss [f], Jess F. Adkins [b]

[a] University of St Andrews, St Andrews, UK
[b] California Institute of Technology, Pasadena, CA, USA
[c] CRPG – CNRS, Vandoeuvre-lès-Nancy, France
[d] Institut de Physique du Globe de Paris (IPGP), Sorbonne Paris Cité, University Paris Diderot, CNRS, Paris, France
[e] Institut Universitaire de France, France
[f] Woods Hole Oceanographic Institution, Woods Hole, MA, USA
[g] University of Texas at Austin, Austin, TX, USA
[h] Florida State University, Tallahassee, FL, USA

ARTICLE INFO

Article history:
Received 6 November 2017
Received in revised form 13 May 2018
Accepted 14 May 2018
Available online 6 June 2018
Editor: D. Vance

Keywords:
sulfur
rivers
weathering
pyrite

ABSTRACT

The biogeochemical sulfur cycle is intimately linked to the cycles of carbon, iron, and oxygen, and plays an important role in global climate via weathering reactions and aerosols. However, many aspects of the modern budget of the global sulfur cycle are not fully understood. We present new $\delta^{34}S$ measurements on sulfate from more than 160 river samples from different geographical and climatic regions—more than 46% of the world's freshwater flux to the ocean is accounted for in this estimate of the global riverine sulfur isotope budget. These measurements include major rivers and their tributaries, as well as time series, and are combined with previously published data to estimate the modern flux-weighted global riverine $\delta^{34}S$ as 4.4 ± 4.5‰ (V-CDT), and 4.8 ± 4.9‰ when the most polluted rivers are excluded. The sulfur isotope data, when combined with major anion and cation concentrations, allow us to tease apart the relative contributions of different processes to the modern riverine sulfur budget, resulting in new estimates of the flux of riverine sulfate due to the oxidative weathering of pyrites (1.3 ± 0.2 Tmol S/y) and the weathering of sedimentary sulfate minerals (1.5 ± 0.2 Tmol S/y). These data indicate that previous estimates of the global oxidative weathering of pyrite have been too low by a factor of two. As pyrite oxidation coupled to carbonate weathering can act as a source of CO_2 to the atmosphere, this global pyrite weathering budget implies that the global CO_2 weathering sink is overestimated. Furthermore, the large range of sulfur isotope ratios in modern rivers indicates that secular changes in the lithologies exposed to weathering through time could play a major role in driving past variations in the $\delta^{34}S$ value of seawater.

1. Introduction

The biogeochemical sulfur cycle is intimately linked to the cycles of carbon and oxygen (e.g. Berner and Raiswell, 1983). Reconstructing the sources and sinks of sulfur to the marine environment in the past is thus important for understanding long-term changes in climate and the redox processes operating in Earth's surface environments. The sulfur isotope compositions of these sources and sinks provide a sensitive tracer of the processes that drive the sulfur cycle because there are large isotope fractionations that occur associated with cycling sulfur between oxidized and reduced phases (e.g. Garrels and Lerman, 1984). Microbial sulfate reduction, for instance, imparts a large sulfur isotope fractionation ($\varepsilon \approx 0$ to -70‰ (e.g. Habicht and Canfield, 2001; Sim et al., 2011)), leaving, on average, pyrite and other sulfide-bearing minerals with lower sulfur isotope ratios than seawater and sedimentary sulfate.

Reconstructions of sulfur isotope ratios through geologic time from marine sedimentary rocks have typically been used to infer

* Corresponding author.
E-mail address: ab276@st-andrews.ac.uk (A. Burke).

https://doi.org/10.1016/j.epsl.2018.05.022
0012-821X/

past changes in the burial flux of reduced sulfur (pyrite) relative to the removal of oxidized sulfur in the form of sulfate (evaporite deposits) (Kump and Garrels, 1986). In a simple isotope box model of the marine sulfur reservoir, variations in the isotopic composition of marine sulfate are interpreted as being driven by relative changes in these outputs, while typically assuming that the input of sulfur to the ocean has remained constant through time. Recent work (Halevy et al., 2012), however, has highlighted the need to consider changes in the flux and the isotopic composition of sulfur to the ocean. Riverine sulfur is the major source of sulfate to the ocean, supplying approximately 4.7 Tmol/y today (including 1.3 Tmol/y from anthropogenic sources (Meybeck, 2003)). Thus in order to fully understand the secular changes in the $\delta^{34}S$ value of seawater, we need to better constrain both the modern values for, and controls on, the isotopic composition of riverine sulfate.

The modern riverine sulfur isotopic composition can also inform estimates of chemical weathering fluxes, with important implications for the carbon cycle. Sulfur isotopes in rivers can provide insight into how much riverine sulfate is sourced from dissolution of sedimentary sulfate minerals versus oxidative weathering of pyrite (OWP) (Calmels et al., 2007). OWP produces sulfuric acid, which is a source of acidity for chemical weathering and which, when it interacts with carbonate minerals, can lead to a net release of CO_2, in contrast to the sink of CO_2 associated with silicate weathering (e.g. Calmels et al., 2007; Torres et al., 2015, 2016). Previous estimates of global OWP fluxes range from 0.5 to 0.65 Tmol/y (Francois and Walker, 1992; Berner and Berner, 1996; Lerman et al., 2007). However, recent studies that use sulfur isotopes (and sulfate-oxygen isotopes) from individual catchments indicate that estimates of global OWP flux are potentially much too low. The sum of OWP fluxes (0.15 Tmol/y) from just three river basins (Mackenzie (Calmels et al., 2007), Kaoping (Das et al., 2012), and Jialing (Li et al., 2011)) can account for a third of previous global OWP flux estimates, despite covering less than 2% of global land area (Das et al., 2012). Underestimating global OWP by this magnitude may result in substantial overestimates of the modern-day sink of CO_2 associated with chemical weathering.

1.1. Previous estimates of $\delta^{34}S$ of river water

Previous estimates of the global sulfur isotopic composition of rivers come from either measurements of river water from a single geographical region (Ivanov et al., 1983) or back-of-the-envelope calculations based on simple geochemical assumptions (Berner and Berner, 1996). The previous data-based study that included the largest amount of river data was limited to the Eurasian continent, and reported an average riverine $\delta^{34}S$ of 9.2‰ (Ivanov et al., 1983). The rivers sampled represent only 7% of the total global riverine discharge and have a total sulfate flux of 0.4 Tmol/y, accounting for only 9% of the total riverine sulfate flux. The limited geographic extent of this estimate raises the question of how representative the value of 9.2‰ is for the global riverine $\delta^{34}S$ input to the oceans, especially given that many of the rivers sampled are weathering large evaporitic deposits of Cambrian/Ordovician age that are exposed across the Siberian Platform (Ivanov et al., 1983; Huh et al., 1998b). These deposits might bias the riverine $\delta^{34}S$ to high values, since evaporites have $\delta^{34}S$ values reflecting the seawater $\delta^{34}S$ during the time of deposition, and range from between 10‰ to 30‰ (e.g. Kampschulte and Strauss, 2004).

Geochemical calculations tend to form the basis of the most commonly cited sulfur isotope compositions for modern riverine sulfate. Isotope mass balance models of the sulfur cycle have typically employed a riverine $\delta^{34}S$ value of around 7–8‰ (e.g. Garrels and Lerman, 1984; Kump and Garrels, 1986; Kurtz et al., 2003; Halevy et al., 2012). These values can be traced back to assumptions about the relative contributions of sulfide and sulfate weathering to the riverine sulfate budget. Specifically, it was assumed that the abundance of sedimentary sulfate minerals is equal to the abundance of sedimentary sulfide minerals and that gypsum weathers twice as fast as pyrite (Berner and Berner, 1996). These two assumptions imply that sulfate mineral weathering should contribute twice as much sulfate to rivers as pyrite weathering. Thus, if a $\delta^{34}S$ value of 17‰ is assumed for sulfate in evaporite minerals and a $\delta^{34}S$ value of −12‰ is assumed for pyrite, then a simple river isotope mass balance predicts an average riverine $\delta^{34}S$ of between 7 to 8‰ (ignoring anthropogenic and other minor sources of sulfate to rivers). It is important to note that because these calculations assumed a fixed ratio of riverine sulfur from sulfide weathering to sulfate weathering, this isotopic composition cannot then be used to calculate the relative proportion of sulfide weathering.

Given the large uncertainties in these estimates of the relative fluxes in the modern biogeochemical sulfur cycle, and the resulting implications for weathering and the modern carbon cycle, the aims of this paper are to: (1) re-evaluate the modern global sulfur isotopic composition of riverine sulfate, and (2) estimate the modern flux of pyrite-derived sulfate supplied to the ocean from rivers using two different and complementary methods: a weathering end-member decomposition and a simple sulfur isotope mass balance.

2. Methods

2.1. Measurement of river water sulfate and $\delta^{34}S$

River waters were sampled either opportunistically or as part of a number of field campaigns between years 1993–2013. Details of all rivers measured in this study for sulfur isotopes can be found in Supplementary Table 1. Previously published sulfur isotope data from main stems of rivers were compiled from the literature, and can be found in Supplementary Table 2, along with the new main stem data from this study. The locations of the main stems of rivers included in this study can be seen in Fig. 1.

The concentration of sulfate in river waters was determined by ion chromatography with a Dionex ICS-2000, using an AS-19 column and 20 mM KOH eluent at the Environmental Analysis Center at Caltech. River samples were then dried down and re-dissolved in 0.01 M HCl. The sulfate was purified from its matrix with an anion exchange column as described in Paris et al. (2014).

New measurements of sulfur isotopes in rivers were made by MC-ICP-MS on a Neptune Plus at Caltech (Paris et al., 2013). Measurement by MC-ICP-MS reduces sample size requirements by three orders of magnitude over traditional gas source mass spectrometric methods, and thus only 20 nmol of sulfate were needed for each sample. Typical rivers have micromolar concentrations of sulfate, thus sample sizes were in the range of 100 µL to a few mL of river water depending on concentration. An in-house sodium sulfate solution was used as a bracketing standard on the MC-ICP-MS to correct for instrumental mass bias. Consistency in chemical preparation and isotope measurement was monitored with multiple full replicates of a seawater standard (21.04 ± 0.17‰ V-CDT 2 s.d.; $n = 20$) and an in-house consistency standard from a filtered river water sample collected from the headwaters of the Arroyo Seco in Angeles National Forest, California near Switzer Falls (4.11 ± 0.24‰ V-CDT 2 s.d.; $n = 10$).

Complete chemistry blanks were monitored along with every set of 10 samples, and contained an average of 0.1 nmol of sulfate. As the smallest samples measured had 20 nmol of sulfate, the blank contamination contributes at most 0.5% of the total sulfate measured, and typically contributes closer to 0.1%, as most samples were analyzed with at least 100 nmol of sulfate. The $\delta^{34}S$ value of the blank is typically close to zero, with a long-term average for

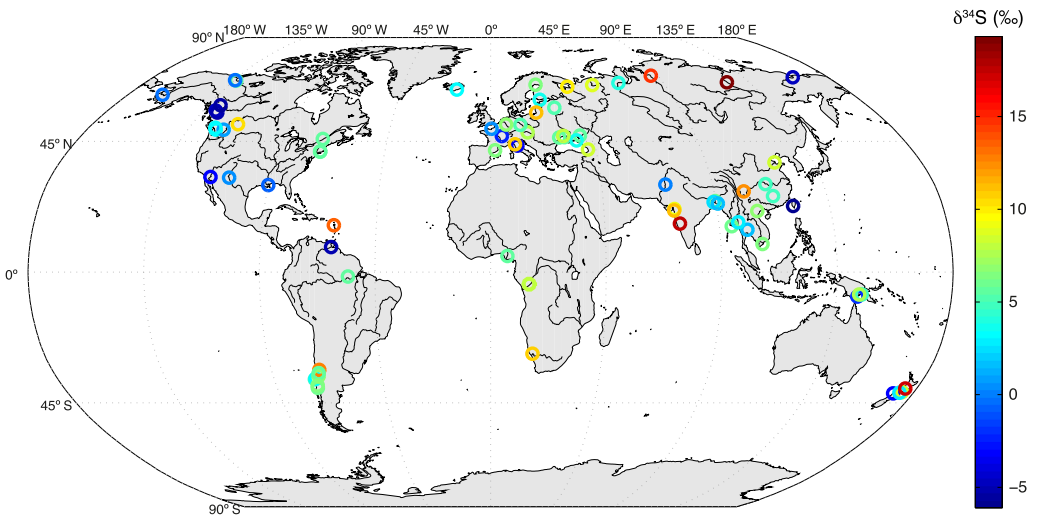

Fig. 1. Global map of measured and compiled main stem river $\delta^{34}S$ values (‰, V-CDT) that contribute to the global flux-weighted average of 4.4‰. The variation seen between these major rivers relates to differences in catchment geology.

all blanks of 2.4 ± 6.5‰ (2 s.d.; $n = 16$). The measured $\delta^{34}S$ of all river samples have been blank corrected with the average of all blanks, and the uncertainty on both the amount of blank and its isotopic ratio is propagated through to the final uncertainties on the riverine $\delta^{34}S$ values.

Global average $\delta^{34}S$ values were calculated based on the data in Supplementary Table 2. Sulfate fluxes were calculated for these main stem rivers by multiplying sulfate concentration by discharge, and these fluxes were used to calculate the global flux-weighted average and standard deviation of $\delta^{34}S$.

2.2. End-member weathering calculation

Previous studies have used coupled $\delta^{34}S$ and $\delta^{18}O$ in sulfate to estimate OWP fluxes in individual river catchments (e.g. Karim and Veizer, 2000; Calmels et al., 2007; Turchyn et al., 2013). These estimates do not rely on knowing the $\delta^{34}S$ of the pyrite being weathered which can have a large range within an individual basin (e.g. Calmels et al., 2007). This is a very powerful technique, but measurement by gas source mass spectrometry requires larger sample sizes and has only been used on a few rivers, in contrast to the numerous $\delta^{34}S$ measurements on riverine sulfate that have been previously published. Thus, to maximize the number of rivers included in our global database (Supplementary Table 2), we used riverine $\delta^{34}S$ and major anion and cation concentrations in an end-member weathering calculation following Gaillardet et al. (1999) to further constrain the global budget of sulfide weathering.

Rivers that were either measured or compiled for $\delta^{34}S$ that also had Cl, Na, Mg, Ca, and Sr concentration data (42 rivers total, representing 41% of the global riverine discharge) were included in this end-member decomposition. A correction for atmospheric deposition from rainwater was made following Gaillardet et al. (1997) based on the Cl concentration of the river. Each river was assigned a critical value of Cl (ranging from 20 to 100 µM, Supplementary Table 2) based on the evapotranspiration factor of the river basin or nearby rivers calculated from the GEMS-GLORI database (Meybeck and Ragu, 1995), and typical values of Cl concentration in rainwater (14 µM, Moller, 1990). If the concentration of Cl in the river was less than the critical value of Cl, then all of the Cl in that river was attributed to rainwater and typical rainwater ratios of Na to Cl (1.15) were used to determine the rainwater-derived fraction of Na for that river. The remaining Na in the river was assumed to come from the weathering of silicates, carbonates, and evaporites. If the concentration of Cl in the river was greater than the critical value, it was assumed that the contribution of Cl from rainwater was equal to the critical value for that river, with the remaining Cl sourced from evaporites. Following the approach of Gaillardet et al. (1999), we then used a series of linear equations to solve for the proportions of sodium in the river that are attributed to evaporite, carbonate, and silicate weathering. The linear equations for each river were solved 10,000 times using a random sampling of weathering end-member values from a normal distribution of the values and associated uncertainties listed in Table 1. The median and standard deviation of these Monte Carlo simulations were used as the end-member fraction and uncertainty for each river (see Supplementary Information).

Table 1
End-member molar ratios (±2 s.d.).

Molar ratio	Rain	Silicate	Carbonate	Evaporite
Ca/Na	0.023 ± 0.01	0.35 ± 0.25	60 ± 30	0.5 ± 0.5
Mg/Na	0.11 ± 0.01	0.25 ± 0.2	30 ± 15	0.1 ± 0.08
Sr/Na	0.0002 ± 0.0001	0.003 ± 0.001	0.04 ± 0.02	0.003 ± 0.002
Cl/Na	1.15 ± 0.1	–	–	1 ± 0.2
S/Na	0.06 ± 0.01	0.019 ± 0.005	0.06 ± 0.03	0.4 ± 0.2

We calculated the proportion of sulfate that could be attributed to each end-member using the S/Na in the end-members (Table 1) and the S/Na measured in the rivers following equation (1):

$$S_i = \frac{(\frac{S}{Na})_i \alpha_i}{(\frac{S}{Na})_{riv}} \quad (1)$$

where (S/Na) are molar ratios of sulfur to sodium, the subscript i refers to the silicate, evaporite, carbonate, and rainwater end-members (Table 1), the subscript *riv* refers to the riverine molar ratio, α is the fraction of sodium attributed to each of the end-members (i) from the end-member weathering calculation, and S_i is the fraction of sulfate in the river attributed to each of the end-members (i). Any sulfate that cannot be attributed to one of the four end-members, we call "excess sulfate". We used Monte Carlo simulations using the end-member values and uncertainties from Table 1 as described above.

Results of this calculation are sensitive to the end-member ratios selected, especially for evaporites, which can vary widely. We use the Ca/Na, Mg/Na, and Sr/Na end-member ratios for silicates and carbonates from Gaillardet et al. (1999) and Negrel et al. (1993), and rainwater ratios from Berner and Berner (1996) and Gaillardet et al. (1999). For evaporites, we calculate mo-

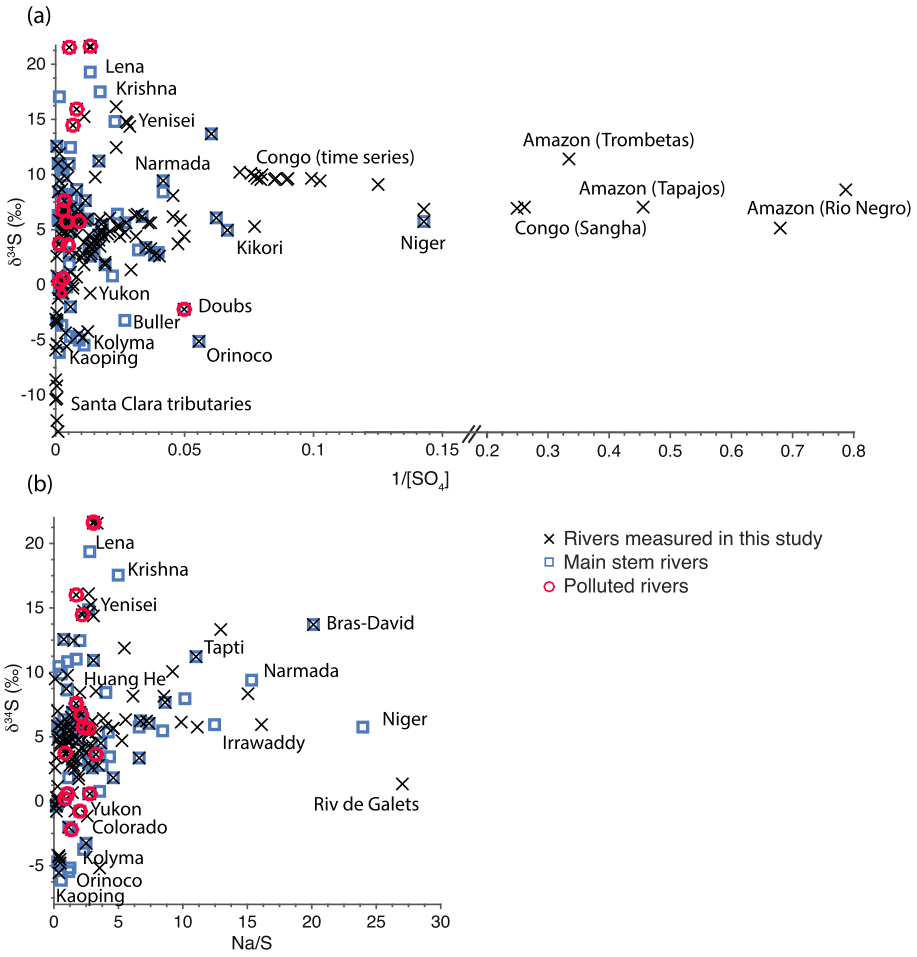

Fig. 2. (**a**) δ^{34}S values (‰, V-CDT) of all rivers measured versus the inverse concentration (μM^{-1}) of sulfate (black x). Rivers designated as main stem rivers (compiled or measured) are shown as blue squares. Rivers identified as being polluted (section 4.1) are circled in red. Note the change in scale on the X-axis after the break. (**b**) Same as above but plotted against the Na/S molar value of the riverine dissolved load. (For interpretation of the colors in the figure(s), the reader is referred to the web version of this article.)

lar ratios based on mineral abundances in evaporites given in Lerman et al. (2007), assuming congruent weathering of evaporites. These evaporite based ratios are consistent with the median ratio calculated from rivers that drain evaporites (Meybeck, 1979, 1984), giving additional support for our choice of end-members.[1] The S/Na value for carbonates is based on the S/Ca molar ratio of 0.001 in marine carbonates (Volkov and Rozanov, 1983) and the Ca/Na value of carbonates of 60 (Negrel et al., 1993). Finally, the S/Na value of the silicate end-member is calculated from global estimates of the abundance of S and Na_2O in continental igneous and metamorphic rocks (Holser and Kaplan, 1966; Rudnick and Gao, 2003). This estimate of S/Na in silicate rocks deliberately does not include sedimentary sulfides (e.g. from shales). Consequently, any sulfate derived from oxidative weathering of sedimentary pyrite would be incorporated into the excess sulfate parameter described above.

3. Results

The river waters analyzed in this study yield a large range of δ^{34}S values, between −13.4‰ and 21.7‰ (Figs. 1 and 2), and represent more than 46% of the global water discharge to the ocean (3.88×10^4 km^3/y, Peucker-Ehrenbrink, 2009). This dataset includes smaller tributaries, as well as time series measurements from individual major rivers (Fraser, Lena, Ob', Yenisei, Yukon, Mackenzie, Kolyma, and Congo rivers). Within an individual river basin, there can be a large range in the δ^{34}S of tributaries. For instance, δ^{34}S values from the Congo River and its tributaries range from 3.7 to 12.5‰ ($n = 7$), those from the Ganges River system range from −1 to 13.3‰ ($n = 3$), and those in the Amazon River basin range from 4.5 to 13.4‰ ($n = 19$), though most of the Amazonian tributaries have a narrow range of 4.5 to 7‰ ($n = 16$), consistent with the findings of Longinelli and Edmond (1983).

The δ^{34}S measured in river time series samples can also show a large range, highlighting temporal heterogeneity in the isotopic composition of riverine sulfate, that is likely driven by varying contributions from tributaries that drain different lithologies (Fig. 3). For instance the δ^{34}S of the Lena River has a range of 7‰ between May and November, the δ^{34}S of the Mackenzie River has a range of 4.5‰ between March and September, and the δ^{34}S of the Fraser River has a range of 5‰ over the course of a year (Supplementary Table 1; Fig. 3). In contrast, time series data from the Congo, Kolyma, Ob', Yenisei, and Yukon rivers have more constant (<2‰ variation) δ^{34}S over the course of several months to a year (Supplementary Table 1).

The flux-weighted average of the rivers gives a δ^{34}S value of 4.4 ± 4.5‰ (1 s.d.). If polluted rivers (identified by having excess chloride relative to sodium concentrations such that ([Na]–[Cl])/[Cl] <

[1] The one exception to this statement is evaporite Mg/Na. The Mg/Na ratio based on mineral abundances is 0.03, while the median Mg/Na ratio from rivers draining evaporites is 0.1. However, the final results are not sensitive to the choice of this parameter, with only a 0.02 Tmol/y difference in the estimate of the global flux of sulfate from evaporites, well within the uncertainty of the calculation (0.2 Tmol/y).

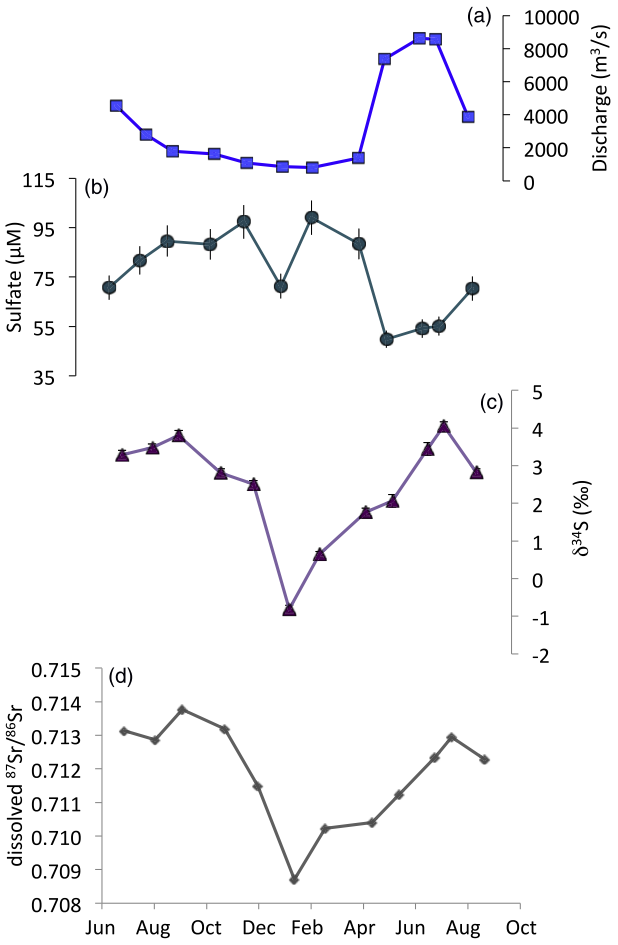

Fig. 3. Time series data from Fraser River samples collected between June 2010 and August 2011. (a) Freshwater discharge (m^3/s), (b) sulfate concentration (μM); (c) $\delta^{34}S$ values (‰, V-CDT), (d) $^{87}Sr/^{86}Sr$ from Voss et al. (2014).

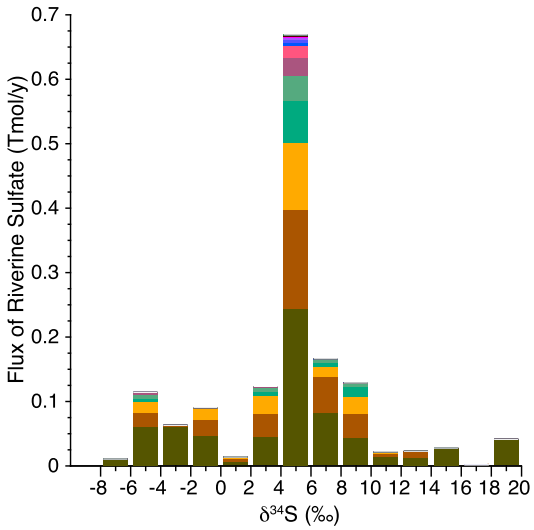

Fig. 4. Stacked bar graph showing the $\delta^{34}S$ values (‰, VCDT) and the flux of sulfate from individual main stem rivers that contribute to the global flux-weighted average $\delta^{34}S$ value of 4.4‰. Each color represents a different river.

0.1; see section 4.1) are excluded[2] from this estimate, the average $\delta^{34}S$ of riverine sulfate is 4.8 ± 4.9‰, and accounts for more than 43% of the water discharge to the ocean. The similarity between these two values suggests that the most polluted rivers do not meaningfully change the estimate of the global riverine $\delta^{34}S$ value. We therefore take the value of 4.8‰ as our best estimate of the modern pre-anthropogenic $\delta^{34}S$ value of river water. The flux-weighted distribution of the isotopic composition of riverine sulfate (Fig. 4) shows that half of the rivers have $\delta^{34}S$ values between 1.8 and 8.2‰ (interquartile range), including the rivers with the largest flux of sulfate (Amazon and Yangtze rivers). Notable exceptions to this include the Mississippi and Lena rivers, which contribute a large flux of sulfate to the oceans, but have low (−5‰) and high $\delta^{34}S$ (19‰) values, respectively.

We can assess how representative our subset of rivers is of global riverine discharge by comparing the flux-weighted Mg/Na and Ca/Na ratios and strontium isotopes from our dataset with global estimates of these values from previously published studies. Our flux weighted Mg/Na ratio of 0.66 and Ca/Na ratio of 1.63 are within the range of previous global estimates of these values of 0.57 to 0.70 and 1.32 to 1.67, respectively (Meybeck and Ragu, 1995; Miller et al., 2011). The same is true if we scale the river fluxes by the large scale drainage regions (Graham et al., 1999; Peucker-Ehrenbrink and Miller, 2007) following Miller et al. (2011). In this case, our subset of rivers yields a Mg/Na ratio of 0.68 and a Ca/Na ratio of 1.70, compared to previously published values of 0.55 to 0.71 and 1.27 to 1.74, respectively (Meybeck and Ragu, 1995; Miller et al., 2011). Thus, our elemental ratios support the use of this subset of rivers for global budget estimates. The flux weighted average $^{87}Sr/^{86}Sr$ ratio from our subset of rivers with published ratios (40% of global water discharge) is 0.7115, slightly higher than estimates of global riverine $^{87}Sr/^{86}Sr$ (0.7111 to 0.7114; Vance et al., 2009; Peucker-Ehrenbrink et al., 2010). The slightly more radiogenic $^{87}Sr/^{86}Sr$ value likely reflects an underrepresentation of younger, more volcanically dominated river basins (e.g. smaller rivers on volcanic islands and along active margins) in our subset of rivers. This might bias our estimate of global riverine $\delta^{34}S$ to higher values, but the effect is likely small given that rivers draining volcanic islands (e.g. Reunion, Iceland) have relatively low concentrations of sulfate (34–70 μM) and have $\delta^{34}S$ values only slightly (1–3‰) lower than our global average (Supplementary Tables 1 and 2).

3.1. Weathering end-member decomposition

End-member decomposition allows us to tease apart the different sources of sulfate to rivers. A plot of $\delta^{34}S$ of riverine sulfate versus the percentage of Na derived from silicate weathering illustrates the importance of pyrite weathering in influencing the sulfur isotopic composition of rivers (Fig. 5). For rivers with no Na derived from silicate weathering, the only other two sources of Na are evaporite and carbonate minerals. As both of these lithologies reflect the sulfur isotopic composition of seawater when they were formed, they should both have high $\delta^{34}S$ values (∼17‰; Holser and Kaplan, 1966). Similarly, for rivers that derive 100% of their Na from silicate weathering (none from evaporites or carbonates), the $\delta^{34}S$ of river water should be similar to the silicate value of 4‰ (Holser and Kaplan, 1966). These two end-members determine the red mixing lines in Fig. 5. Most data plot below these mixing lines, implying a ^{34}S-depleted source of sulfate to the rivers that does not also add Na. The oxidative weathering of sedimentary pyrite could reasonably constitute such a source.

[2] The only river with sufficient data to estimate a pre-anthropogenic, natural $\delta^{34}S$ and flux of sulfate is the Mississippi River. Killingsworth and Bao (2015) used an isotope mixing model to estimate a pre-anthropogenic $\delta^{34}S = -5$‰, and a concentration of sulfate of 115 μM. This pre-anthropogenic estimate is *lower* than the measured $\delta^{34}S = -0.72$‰ and sulfate concentration of 462 μM from this study (which is similar to the isotope and concentration measurements from 2009 to 2013, from Killingsworth and Bao, 2015).

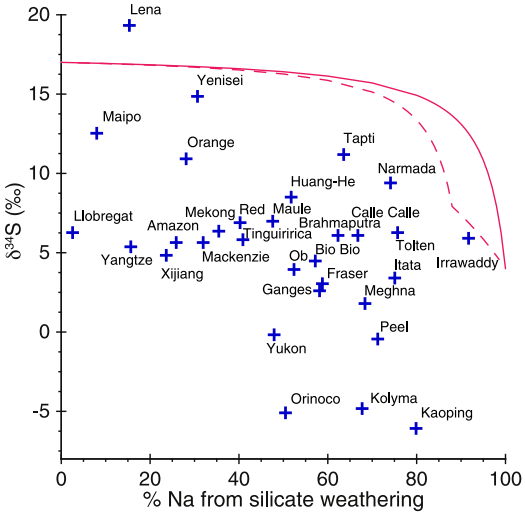

Fig. 5. Riverine δ^{34}S values (‰, V-CDT) of main stem rivers as a function of the percent of Na attributed to silicate weathering from the end-member decomposition. The red solid line is the predicted δ^{34}S based on a riverine isotope mass balance, using the S/Na end-member ratios from Table 1, and assuming that the δ^{34}S value of silicate rocks is 4‰, that the δ^{34}S value of evaporites is 17‰, and that there is no contribution of Na from carbonates. The red dashed line is the predicted δ^{34}S based on a riverine isotope mass balance, using the S/Na end-member ratios from Table 1, and assuming that the δ^{34}S value of silicate rocks is 4‰, that the δ^{34}S value of evaporites and carbonates is 17‰, and that carbonates contribute 12% of the Na (maximum contribution found for all rivers in this study), with the remainder coming from silicates and evaporites.

We further quantify the sources of sulfate to rivers by using the end-member values of S/Na from Table 1 and Equation (1) to convert fractional contributions of Na from the different end-members into fractional contributions of S from the different end-members. Based on our end-member decomposition, evaporite weathering contributes 31 ± 6% (1.5 ± 0.2 Tmol/y) to the global riverine sulfate budget. We find that the contribution of rainwater sulfate to rivers in our database is minor, contributing about 1.6% (0.07 Tmol/y) to the total riverine sulfate flux, consistent with independent estimates of the contribution of cyclic sea salts (0.09–0.13 Tmol/y; Eriksson, 1963; Berner and Berner, 1996) to riverine sulfate. The contribution of carbonate and silicate weathering is also minor with only 0.01 and 0.09 Tmol/y derived from each of those end-members, respectively.

The remaining sulfate in each river that cannot be readily attributed to carbonate, silicate, and evaporite weathering, or to rainwater (sea-salt) constitutes a parameter we call “excess sulfate”. This “excess sulfate” is a combination of the other major sources of sulfate to rivers: pollution, volcanic atmospheric deposition, biogenic emissions, and the oxidative weathering of sedimentary pyrite. This relative contribution of excess sulfate ranges from 0 to more than 97% of the sulfate flux for all rivers, with the exception of the Narmada and Tapti rivers, which have negative excess sulfate values. A negative excess sulfate value implies that the sulfate in those rivers can be more than accounted for by weathering of the three end-members and rainwater inputs, and thus could indicate an unidentified sink for sulfate along the river (e.g. in the river flood plain). For example, from sulfur isotope data it was suggested that removal of riverine sulfate might occur via sulfate reduction and sulfide precipitation in weakly developed soils in the Marsyandi River catchment in the Himalaya (Turchyn et al., 2013). However, the extent to which this process occurs in other river systems remains to be established (Torres et al., 2016). The excess sulfate values thus represent minimum values, and for the remainder of this study we will ignore the two rivers in our compilation that have a negative excess sulfate.

The flux weighted global percentage of excess sulfate is 65 ± 6% (3.1 ± 0.2 Tmol/y), which is dominated by pyrite weathering and pollution. The contributions to riverine sulfate from volcanoes and biogenic emissions are both relatively small (0.34 and 0.14 Tmol/y, respectively; Berner and Berner, 1996). Using an estimate of the pollutive sulfate in rivers of 1.3 Tmol/y (Meybeck, 2003), we estimate that the global contribution of oxidative weathering of pyrite to riverine sulfate is 1.3 Tmol/y, or about 28% of the total sulfate flux from all sources to the ocean (4.7 Tmol/y), and 46% of the flux of sulfate from weathering (i.e. 2.8 Tmol/y, excluding sulfate from pollution, volcanoes, biogenic emissions, and cyclic sea salts).

4. Discussion

4.1. Controls on riverine sulfate δ^{34}S

The highest δ^{34}S values measured (14.4 to 21.7‰) come from the Lena and Yenisei rivers which drain the Siberian Platform—a region of large evaporite and carbonate platforms deposited from late Proterozoic through Paleozoic time (Huh et al., 1998b). Since these rocks are abundant in sulfate phases derived from seawater, they are characterized by relatively high δ^{34}S values. The sulfate minerals weather readily, resulting in both high concentrations of sulfate and high δ^{34}S values for these rivers. The lowest δ^{34}S values (−8.5 to −13.4‰) come from tributaries of the Santa Clara River (e.g. Sespe) in Southern California, which weather sandstones, siltstones, and organic-rich shales of the Monterey Formation and equivalent units. Sedimentary evaporites are absent from the underlying strata, and thus sulfate in these rivers is likely dominated by the oxidation of pyrite and organic sulfur molecules, which, due to the biological isotope fractionations associated with sulfate reduction in organic-rich sediments during their diagenesis and lithification, results in lower overall δ^{34}S values. The lowest δ^{34}S values measured in major rivers come from the Orinoco (−5.1‰) and the Kolyma (−4.2 to −5.6‰) rivers, which also drain catchments rich in sedimentary rocks, including black shales (Edmond et al., 1996; Huh et al., 1998a). These examples are consistent with the notion that local lithology plays a key role in setting the sulfur isotopic composition of rivers, and the important role of black shale weathering in the sulfur budget.

Plots of the δ^{34}S versus inverse concentration of sulfate and versus the riverine Na/S ratio (Fig. 2) show a triangular pattern, indicative of at least three end-members contributing to sulfate in rivers. The most sulfate-rich rivers span a wide range of δ^{34}S values (−13 to 21‰), whereas the rivers with the lowest sulfate concentrations cluster tightly between ∼5–10‰. Rivers plotting in the high concentration-high δ^{34}S region, such as the Lena River, are likely dominated by sulfate minerals weathered from evaporites. Gypsum ($CaSO_4$) dissolves easily, and rivers draining evaporitic rocks usually have high concentrations of total dissolved solids, including sulfate. These rivers have Na/S values ranging between 1.7 and 5, consistent with an evaporite end-member.

Rivers plotting in the high concentration-low δ^{34}S region could have sulfate sources dominated by the oxidative weathering of pyrite, which has low δ^{34}S values, or by pollution, which is often cited in the literature as having low or negative δ^{34}S signatures (e.g. Ivanov et al., 1983). We screened for polluted rivers using ancillary anion and cation data (Fiege et al., 2009; Miller et al., 2011; Voss et al., 2014; Peterson et al., 2016). If the value of ([Na] − [Cl])/[Cl] is less than 0.1, then the river is considered polluted. The main sources of Cl to rivers are sea salt aerosols, evaporites, and pollution. As both sea salt aerosols and evaporites deliver Na and Cl in roughly equal proportions, an excess of Cl relative to Na may be indicative of a polluted river. The following rivers have high

Cl relative to Na: Connecticut, Danube, Indus, Doubs, Lena, Mississippi, Neman, Rhine, Seine, and St. Lawrence. These rivers are also located near large human populations or near industrial centers. The one exception to this is the Lena River, which is influenced by Cl-rich brines (Gaillardet et al., 1999). As shown in Fig. 2, the polluted rivers tend to have high sulfate concentrations (>100 μM, with the exception of the Doubs whose main sulfate sources are atmospheric (Calmels et al., 2014)). However, there is a large range of δ^{34}S for these rivers; thus they do not simply populate the bottom left of the graph, as would be expected if pollution always had a low δ^{34}S signature. Indeed, measurements of δ^{34}S on oil, gas, coal and sulfide ores range from −25 to +30‰ (Newman et al., 1991), and δ^{34}S of fertilizers, another anthropogenic sulfate source, can range from −6.5 to 20.7‰ (Vitoria et al., 2004; Szynkiewicz et al., 2011). Since pollution cannot be the sole reason for the high sulfate concentration and low δ^{34}S, it follows that the oxidation of pyrite is a major source of sulfate to these rivers. This is consistent with the abundance of shales and pyrites in the catchment areas of the rivers (e.g. the Kolyma (Huh et al., 1998a), Orinoco (Edmond et al., 1996), Buller (Robinson and Bottrell, 1997), Kaoping (Das et al., 2012), Skeena (Spence and Telmer, 2005), and Stikine rivers (Calmels et al., 2007)).

Rivers and tributaries with low concentrations of sulfate (e.g. Amazon, Congo, and Niger rivers) tend to have δ^{34}S values of 5–10‰ (Fig. 2). The low sulfate concentrations likely reflect the lack of any significant weathering of evaporites or pyrite-rich shales in these drainage basins. Their low concentration of sulfate could also be attributed in part to the large flow of water and the dilution of solutes, as the concentration of total dissolved solids for these rivers is low at 35–59 mg/L (Meybeck and Ragu, 1995). However, the small range of δ^{34}S values indicates a similar source of sulfate to the rivers, leaving us to conclude that silicate weathering of igneous rock and atmospheric deposition of sulfate (sea salts) are the major sources of sulfate to these rivers and tributaries, consistent with previous studies (Negrel et al., 1993; Gaillardet et al., 1997). Rivers with a high ratio of Na/S also plot within this narrower range of δ^{34}S, consistent with a silicate or atmospheric source.

The wide range in δ^{34}S from tributaries from an individual river basin (e.g. Congo, Ganges, Mackenzie) highlights the spatial heterogeneity of sulfur sources to rivers, that is most likely controlled by heterogeneity of the bedrock geology—and commensurate differences in the isotopic composition of the sulfur-bearing phases—in their catchments. The differences in the temporal variability of δ^{34}S between individual river basins indicate that some rivers (e.g. Lena, Mackenzie, and Fraser) have weathering conditions that are more heterogeneous than other river basins with more constant δ^{34}S, and that the varied lithologies in these river catchments contribute differently to the dissolved load at distinct times throughout the year. For instance, in the case of the Fraser River (Fig. 3), the δ^{34}S of sulfate over the course of a year shows a strong correlation ($r^2 = 0.88$) with the dissolved ^{87}Sr/^{86}Sr ratio in these waters (Voss et al., 2014). Dissolved ^{87}Sr/^{86}Sr values decrease along the flow path of the Fraser River reflecting the underlying geology, as the river flows from Precambrian/Paleozoic sedimentary rocks of the Rocky Mountains, through the young, magmatic and metamorphic rocks of the Coast Range (Cameron and Hattori, 1997). The time series data indicate a greater relative contribution of the Coast Range to the dissolved ion budget during the winter. The sulfur isotope compositions imply that during the winter months, more sulfate is derived from the oxidative weathering of ^{34}S-poor sulfide-bearing phases in the Coast Range, whereas during the summer a greater proportion of the sulfate derives from sulfate minerals within Paleozoic strata.

The importance of pyrite weathering in setting the δ^{34}S value of rivers globally can be seen in Fig. 6. This figure shows the

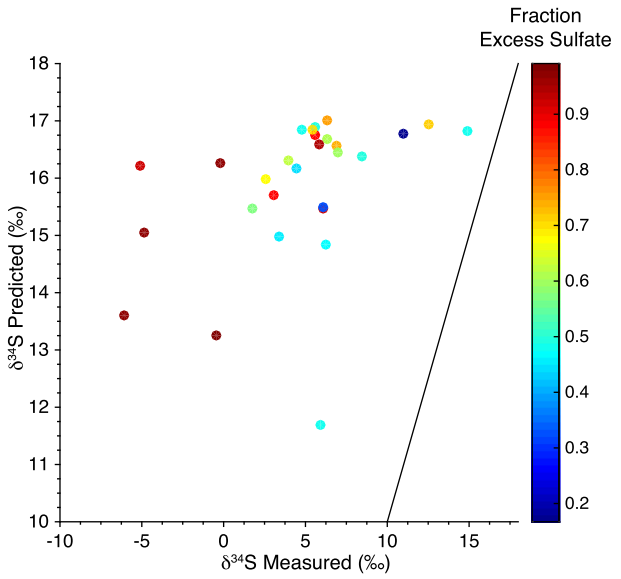

Fig. 6. Plot of predicted δ^{34}S values (based on assumptions of end-members from mixing model, see section 4.1) versus measured δ^{34}S values (‰, V-CDT). The black line is the 1:1 line. The colors indicate the fraction of excess sulfate. Rivers plotting to the left of the line have more negative δ^{34}S values than predicted, and thus are likely influenced by oxidative weathering of pyrite.

relationship between the measured δ^{34}S values versus the δ^{34}S values predicted from a sulfur isotope mass balance in each river based on the weathering end-member decomposition. This sulfur isotope mass balance uses the proportion of sulfate derived from the weathering and rain water end-members and assumes end-member δ^{34}S values of 17‰ for evaporite and carbonate weathering, 4‰ for silicate weathering, and 20‰ for rainwater (Holser and Kaplan, 1966; Herut et al., 1995). The 1:1 line in Fig. 6 indicates rivers whose measured δ^{34}S values can be entirely accounted for by sulfur input from sources besides pyrite weathering and pollution. Most rivers plot to the left of this line indicating that the measured values of δ^{34}S are lower than predicted. Furthermore, the rivers that plot farthest from the line have large excess sulfate proportions (calculated from the end-member decomposition), implying that the sulfur isotopic composition of this excess sulfate has a low δ^{34}S value, consistent with a pyrite source.[3]

4.2. Global dissolved sulfur isotope mass balance for rivers

The riverine δ^{34}S values reported here (4.4 ± 4.5‰ and 4.8 ± 4.9‰ excluding the most polluted rivers) are lower than the previous compilation value from Eurasian rivers of 9‰ (Ivanov et al., 1983) and the values of 7 to 8‰ typically used in models of the global sulfur cycle (e.g. Kump and Garrels, 1986; Kurtz et al., 2003; Halevy et al., 2012). At face value these lower values of the δ^{34}S of rivers imply that a greater fraction of riverine sulfate derives from reduced sources (e.g. pyrite) than previously estimated. This finding is in line with recent studies illustrating the high relative contribution of oxidative weathering of pyrite to riverine sulfate based on detailed studies of individual river basins (e.g. Mackenzie (Calmels et al., 2007), Kaoping (Das et al., 2012), Marysandi (Turchyn et al., 2013), Amazon (Torres et al., 2016) and Ganges–Brahmaputra (Galy and France-Lanord, 1999)), and we can now expand those conclusions to the global budget.

Using a simple terrestrial weathering isotope mass balance akin to that used in Kump and Garrels (1986), we can calculate the fraction of pyrite weathering contributing to riverine sulfate:

[3] Note that the most polluted rivers (see text) have been excluded from these calculations and figures.

$$f_{owp} = -(\delta_{evap} - \delta_{riv})/(\delta_{py} - \delta_{evap}) \quad (2)$$

where f_{owp} is the fraction of pyrite-derived sulfate, δ_{evap} is the $\delta^{34}S$ of evaporite (17‰; Holser and Kaplan, 1966), δ_{riv} is the $\delta^{34}S$ of riverine sulfate (4.8‰, above), and δ_{py} is the $\delta^{34}S$ of pyrite from sedimentary rocks (−12‰; Holser and Kaplan, 1966). This gives a f_{owp} in rivers of 0.42, substantially higher than the estimate of f_{owp} of 0.28 if the riverine $\delta^{34}S$ value is taken to be 9‰ (Ivanov, 1983).

These estimates are very sensitive to the assumption of the end-member $\delta^{34}S$ values of the oxidized (sulfate salts) and reduced (sulfide and disulfide) sedimentary reservoirs, which are difficult to constrain from a global perspective. Estimates of the global $\delta^{34}S$ values of oxidized S in sediments range from 12.1‰ to 19‰, and of reduced sediments from −7.4‰ to −16‰ (Holser et al., 1988 and references therein). These different combinations of δ_{evap} and δ_{py} give a range of f_{owp} between 0.35 to 0.42 (compared to f_{owp} = 0.16 to 0.29 if the river $\delta^{34}S$ value is taken to be 9‰), with a median f_{owp} of 0.41. Despite the large uncertainties in the correct end-member isotope values, the estimate of f_{owp} = 0.41 is broadly consistent with the independently derived fluxes from the weathering end-member decomposition that indicate that pyrite weathering contributes up to 46% of the sulfate flux in rivers due to weathering. The weathering end-member decomposition is based solely on major ion concentrations and not isotope values, and so is independent of the isotope mass balance calculation in Equation (2).

4.3. Implications for the modern sulfur cycle and marine isotope mass balance

Our flux estimate of riverine sulfate from evaporite weathering (1.5 Tmol/y) that we derived from weathering end-member decomposition is larger than the assumed value of 1 Tmol/y of sulfate weathering by Berner and Raiswell (1983) and Garrels and Lerman (1981), which is widely used in box models of the sulfur cycle and is smaller than the value estimated more recently by Lerman et al. (2007) (1.98 Tmol/y). Our estimate of the sulfide weathering flux from the weathering end-member decomposition (1.3 Tmol/y) is about twice as large as the commonly cited estimates of the global OWP flux (0.5–0.64 Tmol/y; Berner and Berner, 1996; Lerman et al., 2007), and is consistent with our estimate from an isotope mass balance discussed in the previous section that is based on the revised global average riverine $\delta^{34}S$ value of 4.8‰. Thus the isotope and river chemistry data independently imply a larger contribution of oxidative weathering of pyrite to the riverine sulfate flux than previously estimated.[4]

It can be informative to investigate the derivation of previous estimates of the sulfate flux from OWP in order to understand why they were significantly lower than our new value. Previous estimates of global OWP from Berner and Berner (1996) and Lerman et al. (2007) both relied on assumptions of the relative abundance of pyrite in sedimentary rocks, though they do this differently. The 0.5 Tmol/y estimate (Berner and Berner, 1996) assumed that the riverine ratio of calcium from weathering of sedimentary rocks to pyrite-derived sulfate must be the same as the ratio of calcium to pyrite sulfur in common sedimentary rocks (which was taken to be 8.5 and 0.3 weight % of calcium and pyrite-S, giving a molar pyrite-S/Ca ratio of 0.04; Garrels and Lerman, 1984). The molar ratios of excess sulfate/Ca from our end-member decomposition are more typically around 0.1 and can be as high as 0.6 for catchments with abundant shales (e.g. Kolyma (Huh et al., 1998a), Orinoco (Edmond et al., 1996), and Kaoping (Das et al., 2012)). Thus the assumed ratio of calcium to pyrite sulfur in common sedimentary rocks might not fully account for the presence of pyrite-rich shales. The OWP flux estimate of 0.64 Tmol/y (Lerman et al., 2007) assumes that 24% of sedimentary sulfur is in the reduced form of pyrite. This percentage is significantly lower than previous estimates, which are closer to 50% (e.g. Holser et al., 1988 and references therein). Thus both of these prior studies potentially underestimated the global abundance of pyrite sulfur in sedimentary rocks by a factor of two, which could help to explain the underestimation of global OWP fluxes.

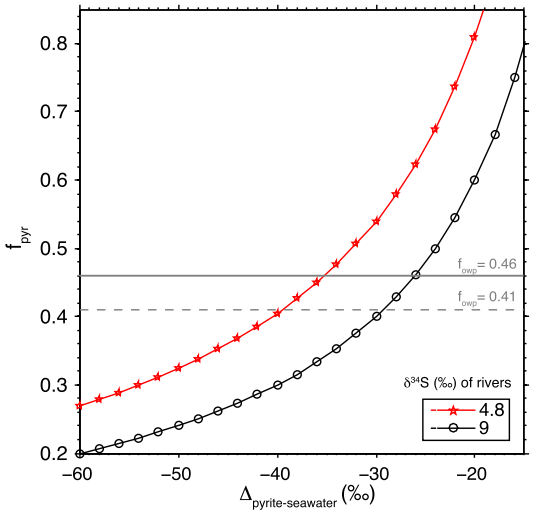

Fig. 7. Sensitivity of the proportion of sulfur buried in marine basins as pyrite (f_{pyr}) as a function of the fractionation ($\Delta_{pyrite\text{-}seawater}$, ‰) between reduced and oxidized sulfur for a given riverine sulfate $\delta^{34}S$ value, and assuming steady state isotope mass balance in the ocean. The red line with stars represents our estimate of the modern riverine $\delta^{34}S$ value from this study (4.8‰). Previous compilations of the riverine $\delta^{34}S$ value were higher (~9‰, black circles; Ivanov et al., 1983). Estimates of the relative contribution of weathering of pyrite (f_{owp}) to modern riverine sulfate from our two independent approaches are shown for reference (f_{owp} = 0.46 (solid line, based on our weathering end-member decomposition from major ion chemistry of the rivers) and f_{owp} = 0.41 (dashed line, based on riverine isotope mass balance)).

Our revised estimate of the OWP flux is similar to the estimate of global pyrite burial in ocean sediments calculated from estimates of global organic carbon burial and the C/S value in modern sediments (1.22 Tmol/y; Berner, 1982). It is also similar to the upper range of estimates of pyrite burial (36% of the total natural, pre-anthropogenic flux) based on marine isotope mass balance and constraints from marine $\delta^{33}S$ (Tostevin et al., 2014). Our upward revision of global pyrite weathering brings the oceanic input and output of reduced sulfur, which previously differed by a factor of 2, into close agreement.

The uncertainties on these modern fluxes from the weathering end-member decomposition of river anion and cation concentration data are still too large (0.2 Tmol/y) to assess whether the modern sulfur cycle is in steady state with regard to the relative amounts of oxidized and reduced sulfur that are weathered and buried. However, if we assume steady-state, our new riverine $\delta^{34}S$ value can be used in a marine isotope mass balance that solves for the fraction of the sulfate removed from the ocean through pyrite burial (f_{pyr}):

$$f_{pyr} = (\delta_{riv} - \delta_{sw})/\left(\Delta^{34}{}_{pyrite\text{-}seawater}\right) \quad (3)$$

where δ_{sw} is the $\delta^{34}S$ of seawater (21‰; Paris et al., 2013) and $\Delta^{34}{}_{pyrite\text{-}seawater}$ is the isotope fractionation between seawater sulfate and sedimentary pyrite in the modern ocean ($\delta_{py} - \delta_{sw}$).

[4] In order to close the riverine sulfate budget, previous estimates attributed any remaining sulfate that did not derive from pyrite or evaporite weathering to pollution (e.g. Berner and Berner, 1996), rather than using an independent estimate of sulfate pollution (Meybeck, 2003) as we have done here.

A plot of the solutions to Equation (3) for our new value for δ_{riv} (4.8‰) and the previous value for δ_{riv} (9‰) is shown in Fig. 7 for a range of $\Delta^{34}_{pyrite\text{-}seawater}$. Our lower value of $\delta_{riv} = 4.8‰$ implies that there is a greater fraction of pyrite burial than previously predicted based on a $\delta_{riv} = 9‰$. Using this model to determine a specific value for the modern fraction of pyrite burial is not currently possible because the global average value of $\Delta^{34}_{pyrite\text{-}seawater}$ is difficult to constrain given the large range of $\delta^{34}S$ values measured in modern pyrites.

If, however, we assume that the fraction of pyrite burial (f_{pyr}) is equivalent to the fraction of pyrite weathered (f_{owp}) as calculated either by the weathering end-member decomposition from major ion chemistry (0.46) or riverine isotope mass balance (0.41), then our data suggest that $\Delta^{34}_{pyrite\text{-}seawater}$ should be −35‰ or −39‰, respectively. These estimates are roughly consistent with canonical assumptions of, $\Delta^{34}_{pyrite\text{-}seawater} = -35‰$ (e.g. Garrels and Lerman, 1981), but are much more positive than flux weighted estimates of this value based on pyrite measurements from modern continental shelf, slope, and rise sediments ($\Delta^{34}_{pyrite\text{-}seawater} = -48‰$; Yu Lein et al., 1983). Modeling studies that use constraints from $\delta^{33}S$ also predict a greater difference between the $\delta^{34}S$ values of seawater and bulk pyrite buried ($\Delta^{34}_{pyrite\text{-}seawater} = -56 \pm 5‰$) (Tostevin et al., 2014). These larger offsets in the isotopic composition of seawater and buried pyrite would imply that the fraction of pyrite buried is 0.29 and 0.34 for $\Delta^{34}_{pyrite\text{-}seawater} = -56$ and $\Delta^{34}_{pyrite\text{-}seawater} = -48$, respectively (Fig. 7), significantly less than our two independent estimates of the fraction of pyrite weathered. If correct, these estimates indicate that the biogeochemical sulfur cycle may not be balanced, and that more pyrite is being weathered than is being buried in modern marine sediments. This conclusion would be consistent with recent ice core evidence that shows a decrease in atmospheric O_2 over the past 800,000 years (Stolper et al., 2016). The magnitude of the imbalance between weathering and burial fluxes of reduced carbon and sulfur that is required to explain the long term oxygen trend in ice cores is ∼2% (Stolper et al., 2016); this number is well within uncertainties of the weathering flux estimates (∼0.2 Tmol/y). However, given the large range of estimates of $\Delta^{34}_{pyrite\text{-}seawater}$ more work constraining global $\Delta^{34}_{pyrite\text{-}seawater}$ from modern sediments would help to resolve this issue.

Our increased estimate of global OWP means that the previously published OWP rates from three river basins (Mackenzie (Calmels et al., 2007), Kaoping (Das et al., 2012), and Jialing (Li et al., 2011)) only account for ∼12% (rather than a third) of the total global OWP flux estimate. Nonetheless, the fact that these rivers drain less than 2% of global surface area highlights the heterogeneity of pyrite weathering; simply put, some river basins will contribute disproportionately to the global pyrite weathering budget, based on their tectonic and geological characteristics. The spatial heterogeneity of pyrite weathering thus has important implications for the long-term variations in the $\delta^{34}S$ of riverine input: changes in paleogeography, paleohydrology, eustasy, and the formation and uplift of sedimentary basins will change both the amounts and types of rock exposed to weathering, which in turn will likely change the value of riverine $\delta^{34}S$ input to the oceans through time.

Finally, the increased estimate of the OWP flux has implications for the modern carbon cycle and carbon-weathering feedbacks. As pyrite oxidation coupled to carbonate weathering can provide a source of CO_2 to the atmosphere (e.g. Calmels et al., 2007; Lerman et al., 2007; Das et al., 2012; Torres et al., 2015, 2016), the greater flux of pyrite-derived sulfate indicates a more significant role for this process in the modern biogeochemical sulfur and carbon cycles. Modern weathering and carbon budgets should be reassessed on a global scale to account for an increased global contribution from OWP.

5. Conclusion

We determined the modern $\delta^{34}S$ value of riverine sulfate to be 4.4 ± 4.5‰, based on measurements of rivers that account for more than 46% of global freshwater discharge. Removing highly polluted rivers from the estimate gives a similar $\delta^{34}S$ value of riverine sulfate of 4.8 ± 4.9‰. These $\delta^{34}S$ values are lower than previous estimates of the isotopic composition of riverine sulfate, and imply a greater contribution of pyrite weathering to riverine sulfate than has previously been assumed. An end-member decomposition of weathering sources to these rivers indicates that the relative contributions of evaporite (sulfate) and pyrite (sulfide) weathering to riverine sulfate budgets are ∼1.5 and 1.3 Tmol S/y, respectively. This estimate of pyrite weathering is twice as high as previous estimates, and is consistent with isotope mass balance constraints on the $\delta^{34}S$ of river water that imply that ∼40% of non-anthropogenic riverine sulfate derives from weathered pyrite. Since pyrite oxidation can act as a source of CO_2 to the atmosphere, this new estimate should reduce the global carbon sink attributed to chemical weathering. Basin lithology exerts a strong control on the $\delta^{34}S$ values of riverine sulfate, questioning the validity of assuming constant $\delta^{34}S$ of riverine input to the ocean over geological time. Stratigraphic trends observed in sulfur isotopes in ancient sedimentary rocks might therefore reflect secular changes in the isotopic composition of the riverine inputs, rather than changes in the relative burial of marine pyrite versus sulfate salt evaporites.

Acknowledgements

This research was funded by a Foster and Coco Stanback postdoctoral fellowship and a Marie Curie Career Integration Grant (CIG14-631752) to AB. JFA acknowledges the support of NSF-OCE grant 1340174 and NSF-EAR grant 1349858. WF acknowledges the support of a grant from the David and Lucile Packard Foundation.

Appendix A. Supplementary material

Supplementary material related to this article can be found online at https://doi.org/10.1016/j.epsl.2018.05.022.

References

Berner, E.K., Berner, R.A., 1996. Global Environment: Water, Air, and Geochemical Cycles. Prentice Hall, New York.

Berner, R.A., 1982. Burial of organic carbon and pyrite sulfur in the modern ocean; its geochemical and environmental significance. Am. J. Sci. 282, 451–473. https://doi.org/10.2475/ajs.282.4.451.

Berner, R.A., Raiswell, R., 1983. Burial of organic-carbon and pyrite sulfur in sediments over Phanerozoic time — a new theory. Geochim. Cosmochim. Acta 47, 855–862.

Calmels, D., Gaillardet, J., Brenot, A., France-Lanord, C., 2007. Sustained sulfide oxidation by physical erosion processes in the Mackenzie River basin: climatic perspectives. Geology 35, 1003. https://doi.org/10.1130/G24132A.1.

Calmels, D., Gaillardet, J., François, L., 2014. Sensitivity of carbonate weathering to soil CO_2 production by biological activity along a temperate climate transect. Chem. Geol. 390, 74–86. https://doi.org/10.1016/j.chemgeo.2014.10.010.

Cameron, E.M., Hattori, K., 1997. Strontium and neodynium isotope ratios in the Fraser river, British Columbia: a riverine transect across the Cordilleran orogen. Chem. Geol. 137, 243–253. https://doi.org/10.1016/S0009-2541(96)00168-4.

Das, A., Chung, C.-H., You, C.-F., 2012. Disproportionately high rates of sulfide oxidation from mountainous river basins of Taiwan orogeny: sulfur isotope evidence. Geophys. Res. Lett. 39. https://doi.org/10.1029/2012GL051549.

Edmond, J.M., Palmer, M.R., Measures, C.I., Brown, E.T., Huh, Y., 1996. Fluvial geochemistry of the eastern slope of the northeastern Andes and its foredeep in the drainage of the Orinoco in Colombia and Venezuela. Geochim. Cosmochim. Acta 60, 2949–2974. https://doi.org/10.1016/0016-7037(96)00142-1.

Eriksson, E., 1963. The yearly circulation of sulfur in nature. J. Geophys. Res. 68, 4001–4008.

Fiege, K., Miller, C.A., Robinson, L.F., Figueroa, R., Peucker-Ehrenbrink, B., 2009. Strontium isotopes in Chilean rivers: the flux of unradiogenic continental Sr to seawater. Chem. Geol. 268, 337–343. https://doi.org/10.1016/CHEMGEO4601.

Francois, L.M., Walker, J.C.G., 1992. Modelling the Phanerozoic carbon cycle and climate, constraints from the $^{87}Sr/^{86}Sr$ isotopic ratio of seawater. Am. J. Sci. 292, 81–135. https://doi.org/10.2475/ajs.292.2.81.

Gaillardet, J., Dupré, B., Allegre, C.J., Negrel, P., 1997. Chemical and physical denudation in the Amazon River basin. Chem. Geol. 142, 141–173.

Gaillardet, J., Dupré, B., Louvat, P., Allegre, C.J., 1999. Global silicate weathering and CO_2 consumption rates deduced from the chemistry of large rivers. Chem. Geol. 159, 3–30.

Galy, A., France-Lanord, C., 1999. Weathering processes in the Ganges–Brahmaputra basin and the riverine alkalinity budget. Chem. Geol. 159, 31–60.

Garrels, R.M., Lerman, A., 1981. Phanerozoic cycles of sedimentary carbon and sulfur. Proc. Natl. Acad. Sci. USA 78, 4652–4656.

Garrels, R.M., Lerman, A., 1984. Coupling of the sedimentary sulfur and carbon cycles; an improved model. Am. J. Sci. 284, 989–1007. https://doi.org/10.2475/ajs.284.9.989.

Graham, S.T., Famiglietti, J.S., Maidment, D.R., 1999. Five-minute, 1/2°, and 1° data sets of continental watersheds and river networks for use in regional and global hydrologic and climate system modeling studies. Water Resour. Res. 35, 583–587. https://doi.org/10.1029/1998WR900068.

Habicht, K.S., Canfield, D.E., 2001. Isotope fractionation by sulfate-reducing natural populations and the isotopic composition of sulfide in marine sediments. Geology 29, 555–558. https://doi.org/10.1130/0091-7613(2001)029<0555:IFBSRN>2.0.CO;2.

Halevy, I., Peters, S.E., Fischer, W.W., 2012. Sulfate burial constraints on the Phanerozoic sulfur cycle. Science 337, 331–334. https://doi.org/10.1126/science.1220224.

Herut, B., Spiro, B., Starinsky, A., Katz, A., 1995. Sources of sulfur in rainwater as indicated by isotopic $\delta^{34}S$ data and chemical composition, Israel. Atmos. Environ. 29, 851–857. https://doi.org/10.1016/1352-2310(94)00307-7.

Holser, W.T., Kaplan, I.R., 1966. Isotope geochemistry of sedimentary sulfates. Chem. Geol. 1, 93–135. https://doi.org/10.1016/0009-2541(66)90011-8.

Holser, W.T., Schidlowski, M., Mackenzie, F.T., Maynard, J.B., 1988. Geochemical cycles of carbon and sulfur. In: Gregor, C.B., Garrels, R.M., Mackenzie, F.T., Maynard, J.B. (Eds.), Chemical Cycles in the Evolution of the Earth. Wiley, New York, pp. 105–173.

Huh, Y., Panteleyev, G., Babich, D., Zaitsev, A., Edmond, J.M., 1998a. The fluvial geochemistry of the rivers of Eastern Siberia: II. Tributaries of the Lena, Omoloy, Yana, Indigirka, Kolyma, and Anadyr draining the collisional/accretionary zone of the Verkhoyansk and Cherskiy ranges. Geochim. Cosmochim. Acta 62, 2053–2075. https://doi.org/10.1016/S0016-7037(98)00127-6.

Huh, Y., Tsoi, M.Y., Zaitsev, A., Edmond, J.M., 1998b. The fluvial geochemistry of the rivers of eastern Siberia: I. Tributaries of the Lena River draining the sedimentary platform of the Siberian Craton. Geochim. Cosmochim. Acta 62, 1657–1676.

Ivanov, M.V., 1983. Major fluxes of the global biogeochemical cycle of sulphur. In: Ivanov, M.V., Freney, J.R. (Eds.), The Global Biogeochemical Sulphur Cycle. John Wiley & Sons, New York, pp. 449–463.

Ivanov, M.V., Grinenko, V.A., Rabinovich, A.P., 1983. The sulphur cycle in continental reservoirs. In: Ivanov, M.V., Freney, J.R. (Eds.), The Global Biogeochemical Sulphur Cycle, Sulphur Flux from Continents to Oceans. John Wiley & Sons, New York, pp. 331–356.

Kampschulte, A., Strauss, H., 2004. The sulfur isotopic evolution of Phanerozoic seawater based on the analysis of structurally substituted sulfate in carbonates. Chem. Geol. 204, 255–286. https://doi.org/10.1016/j.chemgeo.2003.11.013.

Karim, A., Veizer, J., 2000. Weathering processes in the Indus River Basin: implications from riverine carbon, sulfur, oxygen, and strontium isotopes. Chem. Geol. 170, 153–177.

Killingsworth, B.A., Bao, H., 2015. Significant human impact on the flux and $\delta^{34}S$ of sulfate from the Largest River in North America. Environ. Sci. Technol. 49, 4851–4860. https://doi.org/10.1021/es504498s.

Kump, L.R., Garrels, R.M., 1986. Modeling atmospheric O_2 in the global sedimentary redox cycle. Am. J. Sci. 286, 337–360.

Kurtz, A.C., Kump, L.R., Arthur, M.A., Zachos, J.C., Paytan, A., 2003. Early Cenozoic decoupling of the global carbon and sulfur cycles. Paleoceanography 18. https://doi.org/10.1029/2003PA000908.

Lerman, A., Wu, L., Mackenzie, F.T., 2007. CO_2 and H_2SO_4 consumption in weathering and material transport to the ocean, and their role in the global carbon balance. Mar. Chem. 106, 326–350. https://doi.org/10.1016/j.marchem.2006.04.004.

Li, X.D., Liu, C.Q., Liu, X.L., Bao, L.R., 2011. Identification of dissolved sulfate sources and the role of sulfuric acid in carbonate weathering using dual-isotopic data from the Jialing River, Southwest China. J. Asian Earth Sci. 42, 370–380. https://doi.org/10.1016/j.jseaes.2011.06.002.

Longinelli, A., Edmond, J.M., 1983. Isotope geochemistry of the Amazon basin: a reconnaissance. J. Geophys. Res. 88, 3703–3717.

Meybeck, M., 1984. Les fleuves et le cycle géochimique des éléments. (Doctoral dissertation).

Meybeck, M., 1979. Concentrations des eaux fluviales en éléments majeurs et apports en solution aux océans. Rev. Géol. Dyn. Géogr. Phys. 21, 215–246.

Meybeck, M., 2003. Global occurrence of major elements in rivers. In: Drever, J.I. (Ed.), Treatise on Geochemistry. Elsevier, pp. 207–223.

Meybeck, M., Ragu, A., 1995. GEMS/Water Contribution to the Global Register of River Inputs (GLORI). Provisional Final Report. UNEP/WHO/UNESCO, Geneva.

Miller, C.A., Peucker-Ehrenbrink, B., Walker, B.D., Marcantonio, F., 2011. Re-assessing the surface cycling of molybdenum and rhenium. Geochim. Cosmochim. Acta 75, 7146–7179. https://doi.org/10.1016/j.gca.2011.09.005.

Moller, D., 1990. The Na/Cl ratio in rainwater and the seasalt chloride cycle. Tellus, Ser. B 42B, 254–262. https://doi.org/10.1034/j.1600-0889.1990.t01-1-00004.x.

Negrel, P., Allegre, C.J., Dupré, B., Lewin, E., 1993. Erosion sources determined by inversion of major and trace-element ratios and strontium isotopic-ratios in river water — the Congo basin case. Earth Planet. Sci. Lett. 120, 59–76.

Newman, L., Krouse, H.R., Grinenko, V.A., 1991. Sulphur isotope variations in the atmosphere. In: Krouse, H.R., Grinenko, V.A. (Eds.), Stable Isotopes: Natural and Anthropogenic Sulphur in the Environment. John Wiley & Sons, pp. 133–176.

Paris, G., Adkins, J.F., Sessions, A.L., Webb, S.M., Fischer, W.W., 2014. Neoarchean carbonate-associated sulfate records positive ^{33}S anomalies. Science 346, 739–741. https://doi.org/10.1126/science.1258211.

Paris, G., Sessions, A.L., Subhas, A.V., Adkins, J.F., 2013. MC-ICP-MS measurement of $\delta^{34}S$ and $\Delta^{33}S$ in small amounts of dissolved sulfate. Chem. Geol. 345, 50–61. https://doi.org/10.1016/j.chemgeo.2013.02.022.

Peterson, B., Holmes, R.M., McClelland, J.W., Tank, S., Raymond, P.A., 2016. Arctic Great Rivers Observatory 1 Biogeochemistry Data (2009–2011). https://doi.org/10.18739/A2ZQ03.

Peucker-Ehrenbrink, B., 2009. Land2Sea database of river drainage basin sizes, annual water discharges, and suspended sediment fluxes. Geochem. Geophys. Geosyst. 10. https://doi.org/10.1029/2008GC002356.

Peucker-Ehrenbrink, B., Miller, M.W., 2007. Quantitative bedrock geology of the continents and large-scale drainage regions. Geochem. Geophys. Geosyst. 8. https://doi.org/10.1029/2006GC001544.

Peucker-Ehrenbrink, B., Miller, M.W., Arsouze, T., Jeandel, C., 2010. Continental bedrock and riverine fluxes of strontium and neodymium isotopes to the oceans. Geochem. Geophys. Geosyst. 11. https://doi.org/10.1029/2009GC002869.

Robinson, B.W., Bottrell, S.H., 1997. Discrimination of sulfur sources in pristine and polluted New Zealand river catchments using stable isotopes. Appl. Geochem. 12, 305–319. https://doi.org/10.1016/S0883-2927(96)00070-4.

Rudnick, R.L., Gao, S., 2003. Composition of the continental crust. In: Treatise on Geochemistry, vol. 3, pp. 1–64.

Sim, M.S., Ono, S., Donovan, K., Templer, S.P., Bosak, T., 2011. Effect of electron donors on the fractionation of sulfur isotopes by a marine Desulfovibrio sp. Geochim. Cosmochim. Acta 75, 4244–4259. https://doi.org/10.1016/j.gca.2011.05.021.

Spence, J., Telmer, K., 2005. The role of sulfur in chemical weathering and atmospheric CO_2 fluxes: evidence from major ions, $\delta^{13}C_{DIC}$, and $\delta^{34}S_{SO_4}$ in rivers of the Canadian Cordillera. Geochim. Cosmochim. Acta 69, 5441–5458. https://doi.org/10.1016/j.gca.2005.07.011.

Stolper, D.A., Bender, M.L., Dreyfus, G.B., Yan, Y., Higgins, J.A., 2016. A Pleistocene ice core record of atmospheric O_2 concentrations. Science 353, 1427–1430. https://doi.org/10.1126/science.aaf5445.

Szynkiewicz, A., Witcher, J.C., Modelska, M., Borrok, D.M., Pratt, L.M., 2011. Anthropogenic sulfate loads in the Rio Grande, New Mexico (USA). Chem. Geol. 283, 194–209. https://doi.org/10.1016/j.chemgeo.2011.01.017.

Torres, M.A., West, A.J., Clark, K.E., Paris, G., Bouchez, J., Ponton, C., Feakins, S.J., Galy, V., Adkins, J.F., 2016. The acid and alkalinity budgets of weathering in the Andes–Amazon system: insights into the erosional control of global biogeochemical cycles. Earth Planet. Sci. Lett. 450, 381–391. https://doi.org/10.1016/j.epsl.2016.06.012.

Torres, M.A., West, A.J., Li, G., 2015. Sulphide oxidation and carbonate dissolution as a source of CO. Nature 507, 346–349. https://doi.org/10.1038/nature13030.

Tostevin, R., Turchyn, A.V., Farquhar, J., Johnston, D.T., Eldridge, D.L., Bishop, J.K.B., McIlvin, M., 2014. Multiple sulfur isotope constraints on the modern sulfur cycle. Earth Planet. Sci. Lett. 396, 14–21. https://doi.org/10.1016/j.epsl.2014.03.057.

Turchyn, A.V., Tipper, E.T., Galy, A., Lo, J.-K., Bickle, M.J., 2013. Isotope evidence for secondary sulfide precipitation along the Marsyandi River, Nepal, Himalayas. Earth Planet. Sci. Lett. 374, 36–46. https://doi.org/10.1016/j.epsl.2013.04.033.

Vance, D., Teagle, D.A., Foster, G.L., 2009. Variable Quaternary chemical weathering fluxes and imbalances in marine geochemical budgets. Nature 458, 493.

Vitoria, L., Otero, N., Soler, A., Canals, À., 2004. Fertilizer characterization: isotopic data (N, S, O, C, and Sr). Environ. Sci. Technol. 38, 3254–3262. https://doi.org/10.1021/es0348187.

Volkov, I.I., Rozanov, A.G., 1983. The sulfur cycle in oceans. In: The Global Biogeochemical Sulphur Cycle, Reservoirs and Fluxes. John Wiley & Sons, New York, pp. 357–423.

Voss, B.M., Peucker-Ehrenbrink, B., Eglinton, T.I., Fiske, G., Wang, Z.A., Hoering, K.A., Montluçon, D.B., LeCroy, C., Pal, S., Marsh, S., Gillies, S.L., Janmaat, A., Bennett, M., Downey, B., Fanslau, J., Fraser, H., Macklam-Harron, G., Martinec, M., Wiebe, B., 2014. Tracing river chemistry in space and time: dissolved inorganic constituents of the Fraser River, Canada. Geochim. Cosmochim. Acta 124, 283–308. https://doi.org/10.1016/j.gca.2013.09.006.

Yu Lein, A., Grinenko, V.A., Migdisov, A.A., 1983. The sulphur cycle in oceans. In: The Global Biogeochemical Sulphur Cycle, the Mass-Isotopic Balance of Sulphur in Oceanic Sediments. John Wiley & Sons, New York, pp. 423–448.